NRO M33 All Disk Survey of Giant Molecular Clouds (NRO MAGiC): I. HI to H$_2$ Transition

Tomoka TOSAKI[1], Nario KUNO[2], Sachiko ONODERA[2], Rie MIURA[3], Tsyuyoshi SAWADA[4,5]

Kazuyuki MURAOKA[6], Kouichiro NAKANISHI[4], Shinya KOMUGI[4,5], Hiroyuki NAKANISHI[7]

Hiroyuki KANEKO[8], Akihiko HIROTA[2], Kotaro KOHNO[9,10] and Ryohei KAWABE[2]

[1]*Joetsu University of Education, Yamayashiki-machi, Joetsu, Niigata 943-8512, Japan*

tosaki@juen.ac.jp

[2]*Nobeyama Radio Observatory, National Astronomical Observatory of Japan,*

Nobeyama, Minamimaki, Minamisaku, Nagano 384-1305, Japan

[3]*Department of Astronomy, School of Science, The University of Tokyo*

The University of Tokyo, Hongo, Bunkyo, Tokyo 113-0033, Japan

[4]*National Astronomical Observatory of Japan, Osawa, Mitaka, Tokyo 181-8588, Japan*

[4]*Joint ALMA Office, Alonso de C'ordova 3107, Vitacura, Santiago 763-0355, Chile*

[6]*Department of Physical Science, Osaka Prefecture University, Gakuen 1-1, Sakai, Osaka 599-8531,*

Japan

[7]*Graduate School of Science and Engineering, Kagoshima University, 1-21-35 Korimoto,*

Kagoshima, Kagoshima 890-0065, Japan

[8]*The Graduate University for Advanced Studies (Sokendai), Osawa, Mitaka, Tokyo 181-8588, Japan*

[9]*Institute of Astronomy, School of Science, The University of Tokyo,*

Osawa, Mitaka, Tokyo 181-0015, Japan

[10]*Research Center for Early Universe, School of Science, The University of Tokyo,*

Hongo, Bunkyo, Tokyo 113-0033, Japan

Abstract

We present the results of the Nobeyama Radio Observatory (NRO) M33 All Disk ($30' \times 30'$, or 7.3 kpc $\times$ 7.3 kpc) Survey of Giant Molecular Clouds (NRO MAGiC) based on ^{12}CO ($J = 1$–0) observations using the NRO 45-m telescope. The spatial resolution of the resultant map is $19''.3$, corresponding to 81 pc, which is sufficient to identify each Giant Molecular Cloud (GMC) in the disk. We found clumpy structures with a typical spatial scale of $\sim$100 pc, corresponding to GMCs, and no diffuse, smoothly distributed component of molecular gas at this sensitivity. The overall distribution of molecular gas roughly agrees with that of HI. However, closer inspection of the CO and HI maps suggests that not every CO emission is associated with local HI peaks, particularly in the inner portion of the disk ($r < 2$ kpc), although most

1

of CO emission is located at the local Hi peaks in the outer radii. We found that most uncovered GMCs are accompanied by massive star-forming regions, although the star formation rates (SFRs) vary widely from cloud to cloud. The azimuthally averaged Hi gas surface density exhibits a flat radial distribution. However, the CO radial distribution shows a significant enhancement within the central 1–2 kpc region, which is very similar to that of the SFR. We obtained a map of the molecular fraction, $f_{\mathrm{mol}} = \Sigma_{\mathrm{H}_2}/(\Sigma_{\mathrm{Hi}} + \Sigma_{\mathrm{H}_2})$, at a 100-pc resolution. This is the first f_{mol} map covering an entire galaxy with a GMC-scale resolution. We find that f_{mol} tends to be high near the center. The correlation between f_{mol} and gas surface density shows two distinct sequences. The presence of two correlation sequences can be explained by differences in metallicity, i.e., higher ($\sim$2-fold) metallicity in the central region ($r < 1.5$ kpc) than in the outer parts. Alternatively, differences in scale height can also account for the two sequences, i.e., increased scale height toward the outer disk.

Key words: galaxies: individual (M33) – galaxies: ISM – radio lines: galaxies

1. Introduction

The interstellar medium (ISM) is one of the essential components of galaxies because stars are born in and return to them. The ISM is greatly influenced by massive stars due to their stellar winds and supernova after their death. Therefore, the formation process of massive stars within the ISM is crucial for understanding of the nature and evolution of galaxies. In the Milky Way Galaxy, a large fraction of the ISM is in the form of Giant Molecular Clouds (GMCs; Sanders et al. 1985; Scoville & Sanders 1987), and they are known to be major sites of massive star formation (Waller et al. 1987).

At this spatial scale, i.e., a few tens to a hundred pc we can find a wide variety of star-formation activities and the nature of molecular clouds. For example, in the LMC, the variation in star-formation activity from cloud to cloud also becomes visible at this spatial scale, and it is interpreted as indicating different evolutionary stages of GMCs along the star formation processes (Kawamura et al. 2009). Furthermore, no tight correlation between the molecular gas masses and star formation rates (SFRs) can be found among GMCs in M33 seen at a scale of $\sim$100 pc or smaller (Onodera et al. 2010), despite the fact that there exists a tight correlation between the molecular gas masses and SFRs at scales of a few thousand to a few hundred pc in galaxies, known as the Kenicutt–Schmidt law (K-S law; Kennicutt 1998). The reported breakdown of the K-S law in M33 is presumably due to the differences in the star-formation properties, i.e., GMCs at different evolutionary stages (Onodera et al. 2010). With $\sim$100-pc-scale observations of multitransition CO lines, the coexistence of GMCs in various evolutionary stages has also been reported within the supergiant Hii region NGC 604 in M33, suggesting that sequential star formation is on-going (Tosaki et al. 2007; Miura et al. 2010).

Consequently, a survey of GMCs at a spatial scale of $\sim$100 pc is essential for understanding of the processes of massive stars from the ISM.

In addition to this, an unbiased survey is also important because it can sample GMCs in various environments, i.e., in the central region, outer region, spiral arms, inter-arm regions, etc. Formations of GMCs, dense molecular gas, and massive stars will be affected not only by local processes within individual GMCs but also by these global structures of a galaxy or environments within a galaxy.

Furthermore, the transition from atomic gas to molecular gas is also essential to understanding the nature and evolution of the ISM, since the first phase of star formation process is the formation of a dense gas cloud from the diffuse ISM. Many studies of the transition from atomic to molecular gas have been conducted using both theoretical and observational approaches.

Elmegreen (1993) introduced the molecular fraction f_{mol} as a parameter to quantify the transition. It is the ratio of the molecular gas surface density to the total gas surface density including both atomic and molecular gases. f_{mol} can be expressed as a function of metallicity, UV radiation field, and gas pressure. In particular, metallicity is considered to have a strong impact on the transition of a gas from atomic to molecular. Observationally, the presence of a "molecular front," i.e., a sharp transition front from molecular to atomic, has been identified in some nearby galaxies (Honma et al. 1995; Sofue et al. 1995; Nakanishi et al. 2006). This suggests that the transition from atomic gas to molecular gas occurs within a very narrow span along the galactic radius, and the variation in interstellar metallicity has been suggested to play a crucial role in this phase transition (Honma et al. 1995). However, these previous studies on the gas phase transition were based on observations at a resolution of a few hundred pc. It is important to understand the transformation process of the gas phase at the GMC scale, an essential spatial scale for the ISM, in order to obtain a unified picture of the change in the ISM from the diffuse atomic phase to massive stars.

M33 is one of the nearest spiral galaxies in the local group ($D = 840$ kpc; Freedman et al. 1991). The proximity of M33 allows us to resolve the individual GMCs with the existing large-aperture single dishes. Since M33 has a relatively small inclination angle of 51° (Deul & van der Hulst 1987), we can obtain a comprehensive view of a galaxy. This is a key advantage for the study of the correlation between GMC properties and galactic structures such as spiral arms.

There are many previous studies on the ISM and star formation in M33. Whole-disk surveys of molecular gas in the ^{12}CO ($J = 1$–0) line have been conducted with the BIMA interferometer (Engargiola et al. 2003) and FCRAO 14-m telescope (Heyer et al. 2004), and Rosolowsky et al. (2007) combined the results of these data with observations with the 45-m telescope at the Nobeyama Radio Observatory (NRO) toward a part of the disk. A partial mapping of ^{12}CO ($J = 2$–1) has also been conducted with the IRAM 30-m telescope and a

Table 1. Wide-area CO observatons of M33

| transition | telescope | area | resolution | | noise level |
| | | | spatial | velocity | |
		(arcmin^2)	(arcsec)	(km s^{-1})	(mK)
$J=1$–0	BIMA[*]	1100	13	2	240
	FCRAO 14 m[†]	960	50	1	53
	BIMIA + FCRAO 14 m + NRO 45 m[‡]	172	20	2.6	60
	NRO 45 m[§]	900	19	2.5	130
$J=2$–1	IRAM 30 m[‖]	650	12	2.6	20–50

[*] Engargiola et al. 2003

[†] Heyer et al. 2004

[‡] Rosolowsky et al. 2007

[§] this work

[‖] Gratier et al. 2010

comparison between the CO and H I distributions has been made (Gratier et al. 2010). Selected regions of M33, such as the supergiant H II region NGC 604, have also been mapped in ^{12}CO ($J=1$–0) lines using the OVRO array (Wilson & Scoville 1989, 1990) and NMA (Miura et al. 2010), and ^{12}CO ($J=1$–0)/^{12}CO ($J=3$–2) multitransition maps of NGC 604 have been presented using the NRO 45-m and ASTE 10-m dishes (Tosaki et al. 2007). Atomic gas (H I) in M33 has been studied with the VLA and Effesberg 100-m telescope (Deul & van der Hulst 1987), and the cold dust component has been mapped in the 1.1 mm (AzTEC/ASTE; Komugi et al. 2011) and Herschel SPIRE bands (250–500 μm; Kramer et al. 2010), showing a decline in cold dust temperature as a function of radius.

Here we present the initial results of the NRO M33 All Disk Survey of Giant Molecular Clouds (NRO MAGiC) project conducted using the NRO 45-m telescope. By using the largest millimeter-wave telescope equipped with a multibeam receiver system (Sunada et al. 2000) combined with an efficient on-the-fly (OTF) technique (Sawada et al. 2008), we have obtained a sensitive map of ^{12}CO ($J=1$–0) emission over almost the entire region of M33 with a uniform quality of spectra at a GMC-scale spatial resolution. The survey area, sensitivity, and spatial resolution of this map is compared with that of others of M33 in Table 1.

Initial results of the survey (northern half of the map) have already been used to show the breakdown of the K-S law at <100-pc scales (Onodera et al. 2010), emphasizing the importance of ∼100-pc-scale observations of the ISM and star formation.

In this paper, we present an overview of the whole-disk ^{12}CO ($J=1$–0) survey of M33 using the NRO 45-m telescope, with particular focus on the atomic-to-molecular gas phase transition at the GMC scale.

2. Observations

We observed the ^{12}CO ($J = 1$–0) emission toward the disk of M33. Figure 1 shows our observed area, $30' \times 30'$, corresponding to 7.3 kpc $\times$ 7.3 kpc. It covers most of the molecular gas disk and includes many star forming regions.

The observations were conducted from January 2008 to April 2009 using the NRO 45-m telescope equipped with 5×5 focal-plane SIS array receivers (BEARS) capable of simultaneously observing 25 positions in the sky (Sunada et al. 2000). Using a 100-GHz SIS receiver (S100) equipped with a single sideband filter, NGC 7538 was observed to measure the sideband ratio of each beam of BEARS, which consists of double-side-band receivers. The main beam efficiency measured with S100 was $\eta_{\mathrm{mb}} = 0.32 \pm 0.02$ at 115 GHz and the errors in the scaling factors of BEARS were smaller than $\sim$20%. Wide-band digital autocorrelators (AC) were used to cover a velocity width of 1332 km s^{-1} with a velocity resolution of 2.6 km s^{-1} at 115.271204 GHz. We monitored a SiO maser source IRC+30021 with the five-points observation method using a 43-GHz SIS receiver (S40) every 1 h to check the pointing accuracy. Note that the final map was made using data with pointing errors smaller than 7.5$''$ and with wind speeds lower than 10 m s^{-1} to avoid the systematic intensity loss due to the pointing errors. The resultant total observation time was 136 h.

The observations were performed with the OTF mapping technique (Sawada et al. 2008). The "scanning noise" was removed by combining the horizontal and perpendicular scans using basket weaving. The data reductions were made with the OTF reduction software package NOSTAR, which was implemented by the NRO. Although the beam size of the telescope was 15$''$, the spatial resolution of the final map was 19.3$''$ due to the grid spacing of 7.5$''$.

The rms noise levels in the velocity channel map with a velocity range of 2.6 km s^{-1} and the total integrated intensity map were 130 mK and 1.6 K km s^{-1}, respectively, in the main beam temperature scale. The noise level in the integrated intensity map corresponds to $9.6 \times 10^{4} M_{\odot}$ in the beam size (80 pc) by applying the Galactic CO-to-H$_2$ conversion factor, 3×10^{20} cm^{-2} (K km s^{-1})$^{-1}$ (Wilson & Scoville 1990). This value corresponds to a limiting mass surface density of $15 M_{\odot} \mathrm{pc}^{-2}$, including a correction of He, and is much lower than the surface density of GMCs in the Milky Way, 40–$100 M_{\odot} \mathrm{pc}^{-2}$ (Heyer et al. 2009).

3. Results

3.1. Total integrated intensity map and velocity field

Figure 2 shows the total integrated intensity map and intensity-weighted mean radial velocity map of ^{12}CO ($J = 1$–0) emission. This figure reveals many clumps with a typical size of $\sim$100 pc, similar to that of GMCs in the Milky Way (Scoville & Sanders 1987) rather than that of Giant Molecular Associations (GMAs; Rand & Kulkarni 1990). There are chains of such "GMCs" in the northern and southern spiral arms. Note that most of the emission consists of
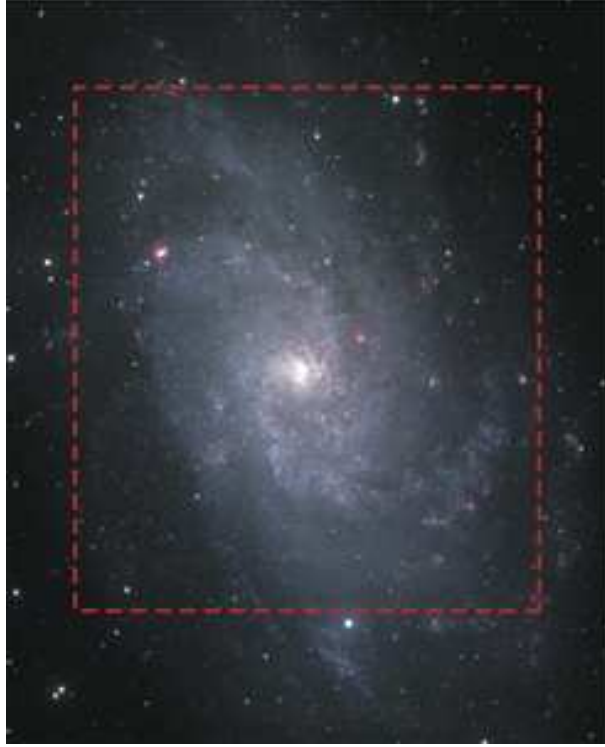
Fig. 1. Observed area (dashed box, $30' \times 30'$) superposed on a three-color composite optical image of M33 obtained with the Subaru telescope: courtesy of V. Vansevicius, S. Okamoto, and N. Arimoto. The optical image consists of three colors, blue (B), green (V), and red (Hα). The Hα image is not continuum-subtracted.

such GMCs and no diffuse emission is seen in the map above the limiting mas surface density of 15 $M_\odot\mathrm{pc}^{-2}$. We see no concentration of CO at the galactic center in this map, unlike in most molecule-rich galaxies (Sakamoto et al. 1999). These properties are consistent with maps obtained by previous studies (Rosolowsky et al. 2007).

The velocity field of the ^{12}CO ($J = 1$–0) emission in figure 2 is similar to that of H$_{\mathrm{I}}$ emission (Deul & van der Hulst 1987), except for a few GMCs (e.g., GMCs located in the southern arm). The velocity field is globally dominated by galactic rotation, and shows no clear evidence for streaming motion along spiral arms, unlike grand design spiral galaxies (e.g., M51; Kuno & Nakai 1997). This is consistent with low amplitude of arm strength in M33 (Regan & Vogel 1994).

3.2. Comparison with atomic gas and SFR

Figure 3 shows CO intensity maps of M33 superposed on the H$_{\mathrm{I}}$ emission (left) and SFR (right). The H$_{\mathrm{I}}$ data of M33 are from observations made with the Westerbork Synthesis Radio Telescope (WSRT) combined those made with the Effelsberg 100-m telescope in order to compensate for the missing short spacings of the WSRT interferometry data (Deul & van der Hulst 1987). The original data, with a resolution of $12'' \times 24''$, was convolved to a resolution of

6
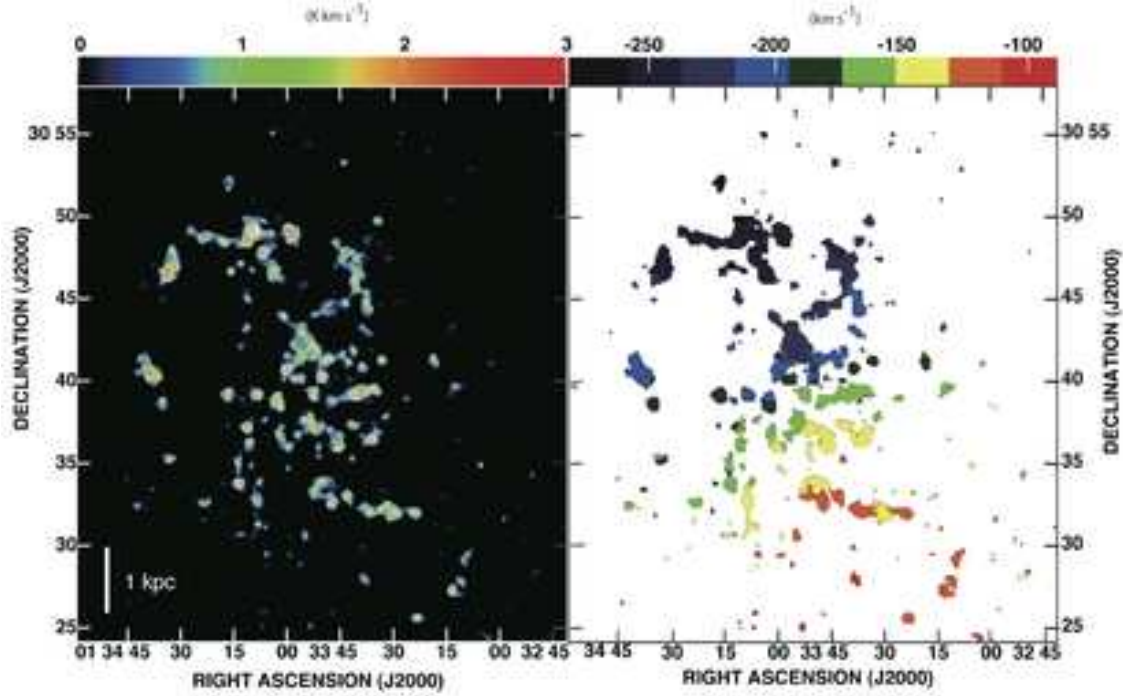
Fig. 2. Total integrated intensity map (left) and intensity-weighted mean radial velocity map (right) of ^{12}CO ($J = 1$–0) emission acquired with the NRO 45-m telescope. The map size is $30' \times 30'$, and the effective spatial resolution is $19''$, corresponding to 7.3 kpc $\times$7.3 kpc and 81 pc at the distance of M33 (D = 840 kpc), respectively. The contour interval is 0.5 K km s^{-1} in the T_a^* scale, corresponding to 1 σ.

$24'' \times 24''$ (Rosolowsky et al. 2007).

The Hi emission map shows a more wide-spread distribution than that of the CO emission, and we found CO emission where Hi emission was distributed. However, we also found different tendencies in the correlation between the CO and Hi distributions for the outer and inner regions of M33: most CO clouds are associated with local Hi peaks in the outer regions, whereas no such clear correspondence can be found in the inner regions.

The SFR was calculated using the relation between the SFR and the extinction-corrected Hα line emission presented by Calzetti et al. (2007). The Hα image of M33 was used by Hoopes & Walterbos (2000). The Multiband Imaging Photometer for Spitzer (MIPS) 24-μm data retrieved by the Spitzer Science Center (Rieke et al. 2004) were used for extinction-correction. The detailed data reduction process for the 24-μm images is explained by Onodera et al. (2010). The calculated SFR is shown on the right in figure 3(b) as a color scale together with the CO emission (contour). This figure shows that most of the GMCs are associated with star-forming regions. However, we also find star-forming regions without GMCs, as well as GMCs without star-forming regions. Among the GMCs associated with star-forming regions, we can see a wide range of star-forming activities: some GMCs show elevated SFRs, whereas others only host calm star-formation activity.
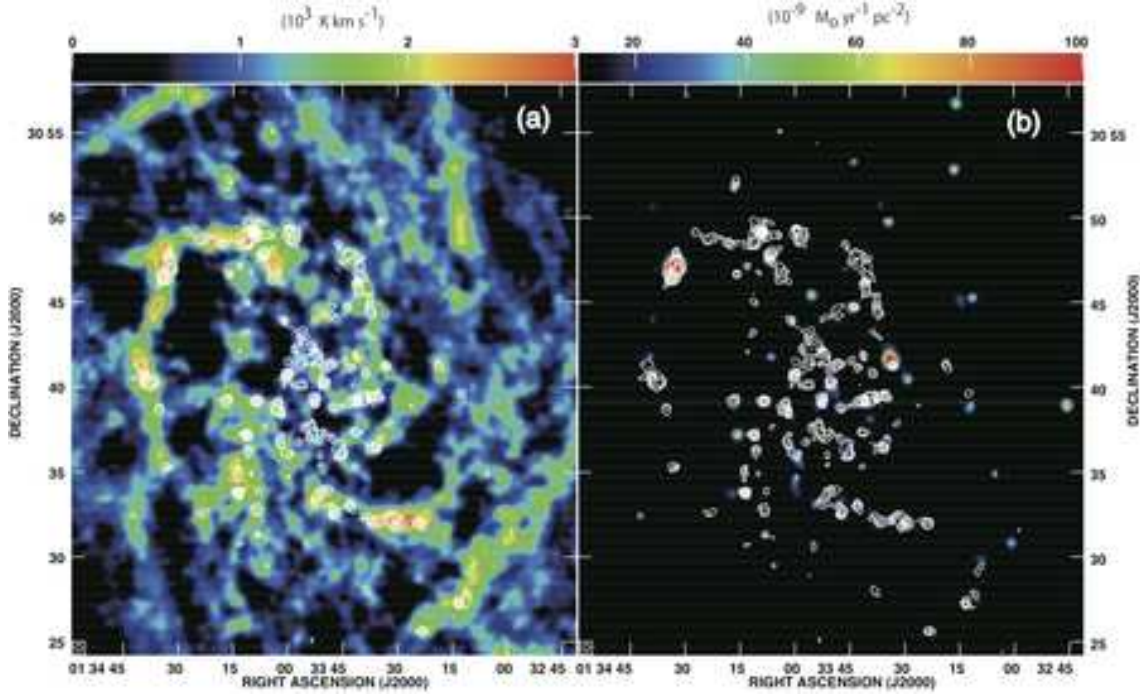
Fig. 3. Total integrated intensity map of ^{12}CO ($J = 1$–0) emission (contours) superposed on HI emission (left, Rosolowsky et al. 2007) and star-formation rate (right) derived from Hα luminosity (Hoopes & Walterbos 2000) with extinction-correction using MIPS 24-μm data (Rieke et al. 2004). The contour interva and lowest contour aew same as figure 2.

3.3. Radial distributions of molecular and atomic gas and SFR

Radial distributions of the molecular and atomic gas surface densities together with SFR are displayed in figure 4. They are de-projected considering the inclination of M33.

We found that the surface density of atomic gas is higher than that of molecular gas at all radii in this figure. This tendency is slightly different from the previous result obtained by Gratier et al. (2010); the molecular gas surface density at central kilopersec is higher than that of the atomic gas in their result, although overall tendency on H$_2$ and HI radial distributions are similar to us. One of the possible causes for this discrepancy can be due to the lower atomic gas surface density estimated based on the only VLA data without the correction of missing flux. The radial distribution of molecular gas surface density shows an overall decline, with two significant local peaks at the radii of 0.1 and 0.5 kpc. By contrast, the surface density of atomic gas is rather flat, although it shows several small peaks. The radial distribution of SFR is similar to that of molecular gas; again, it shows a decline from the center to the outer part of the galaxy, and we also found four local peaks in the radial distribution of SFR, at radii of 0, 0.5, 1, and 3 kpc from the center. The first two peaks near the center correspond to the local peaks in molecular and atomic gas surface densities. The third SFR peak at $r \sim 1$ kpc is associated with a HI peak, but there is no corresponding CO peak.

8
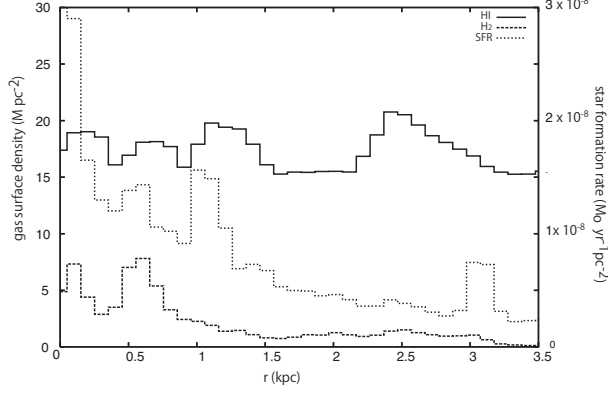
Fig. 4. Radial distribution of the surface densities of H I (solid line), H_2 (dashed line), and star formation rate (SFR; dotted line).

4. Discussion

As mentioned above (Section 3.2), most of the molecular clouds are associated with local H I peaks in the outer regions, whereas no such clear correspondence can be found in the inner regions. This suggests that the process of transition from atomic gas to molecular gas is different in the outer and inner regions and that the process is more efficient in the inner region. To address the issue quantitatively, we derive the fraction of molecular gas to the total gas surface densities (H I + H_2), f_{mol}, which is expressed as follows (Elmegreen 1993; Nakanishi et al. 2006).

$$f_{\mathrm{mol}} = \frac{\Sigma_{\mathrm{H_2}}}{\Sigma_{\mathrm{HI}} + \Sigma_{\mathrm{H_2}}}, \tag{1}$$

where $\Sigma_{\mathrm{H_2}}$ and Σ_{HI} are the molecular and atomic gas surface densities, respectively. Figure 5 shows the distribution of f_{mol} values in the panel on the left. This is the first f_{mol} map covering an entire galaxy with a GMC-scale resolution ($\sim$100 pc). We found that the f_{mol} values range from $\leq$0.1 to 0.6, showing difference among GMCs. This figure also reveals that f_{mol} is higher in the inner region than the outer region. The radial distribution of f_{mol} (figure 6) also confirms this finding: it has two peaks near the center and at a radius of $\sim$0.5 kpc, and decreases toward the outer regions. This suggests that molecular gas is formed more efficiently in the inner region. A sharp decrease in f_{mol} is clearly seen around $r = 1$–1.5 kpc, and we suggest that the molecular front (Sofue et al. 1995; Honma et al. 1995) exists in this region.

The map of f_{mol} is superposed on the SFR map in the panel on the right in figure 5. At the GMC scale, no correlation between H_2 and SFR is seen due to differences in the evolutionary stages of the GMCs (Onodera et al. 2010), and this figure also indicates no correlation between f_{mol} and SFR. It indicates that the fraction of molecular gas in each GMC is not affected by the current star forming activity.

9

f_{mol} is determined by ISM pressure (P), metallicity (Z), and the UV radiation field (U) (Elmegreen 1993; Nakanishi et al. 2006; Honma et al. 1995; Kuno et al. 1995). Here, in hydrostatic equilibrium for gas and star disk, total midplane gas pressure is given as follows (Elmegreen 1989);

$$P = \frac{\pi}{2} G \Sigma_{gas} (\Sigma_{gas} + \Sigma_{star} \frac{c_g}{c_s}). \tag{2}$$

c_g and c_s are velocity dispersions of gas and stars, respectively. Assuming that the distributions of stars and gas are similar, Σ_{star} is proportional to Σ_{gas}. Then, P is proportional to the square of the gas surface density, $\Sigma_{\mathrm{HI+H_2}}$. In other words, f_{mol} can be expressed as a function of Σ for given Z and U.

Figure 7 shows the correlation between $\Sigma_{\mathrm{HI+H_2}}$ and f_{mol}. The red, blue, and green dots indicate the measured data points at the inner ($r \leq 1.5$ kpc), intermediate (1.5 kpc $\leq r \leq 3.0$ kpc), and outer radii ($r \geq 3.0$ kpc), respectively.

We find the presence of two sequences in the $\Sigma_{\mathrm{HI+H_2}}$–f_{mol} correlation in this figure: One is the sequence that can be seen in the upper left part of the figure or in the inner region ($r \leq 1.5$ kpc), showing higher f_{mol} values with respect to a certain $\Sigma_{\mathrm{HI+H_2}}$. The other sequence can be found at the lower right part of the figure, i.e., in the outer region ($r \geq 3$ kpc) of the galaxy, where lower f_{mol} values can be seen compared with the previous $\Sigma_{\mathrm{HI+H_2}}$–f_{mol} sequence. This means that we find two distinct $\Sigma_{\mathrm{HI+H_2}}$ values for a certain f_{mol} value: i.e., the $\Sigma_{\mathrm{HI+H_2}}$ for a given f_{mol} value is higher in the outer part of the galaxy than in the inner part for the same f_{mol}. In other words, for a given gas surface density, f_{mol} value is higher in the inner part than in the outer part. This causes high f_{mol} of GMCs in the inner region shown in figure 6.

Here we investigate the possible causes for the existence of two sequences in the $\Sigma_{\mathrm{HI+H_2}}$–f_{mol} diagram. The first possibility is that molecular gas is formed more efficiently in the inner part of the galaxy. Another possibility is that we are overestimating the gas density in the outer part of the galaxy. Dynamical effects such as shock compression due to spiral arms can also be a possible cause. These three possibilities are examined below.

4.1. Efficient molecular gas formation – metallicity and radiation field

Here we discuss the first possibility. As mentioned above, f_{mol} can be governed by the interstellar radiation field strength U and metallicity Z. If the radiation field strength U is constant over the whole radius, the observed higher f_{mol} value in the inner part of the galaxy can be explained by higher metallicity Z. For instance, the two observed sequences correspond to two distinct metallicities, i.e., $Z = 0.3Z_0$ and $Z = 0.15Z_0$, for the inner and outer parts, respectively, at $U = U_0$. Similarly, $Z = Z_0$ and $Z = 0.5Z_0$ at $U = 10U_0$. Here, U_0 and Z_0 are the values of U and Z in the solar neighborhood, respectively. In short, a difference in Z of a factor of two can explain the two observed sequences if U is constant throughout the galaxy.
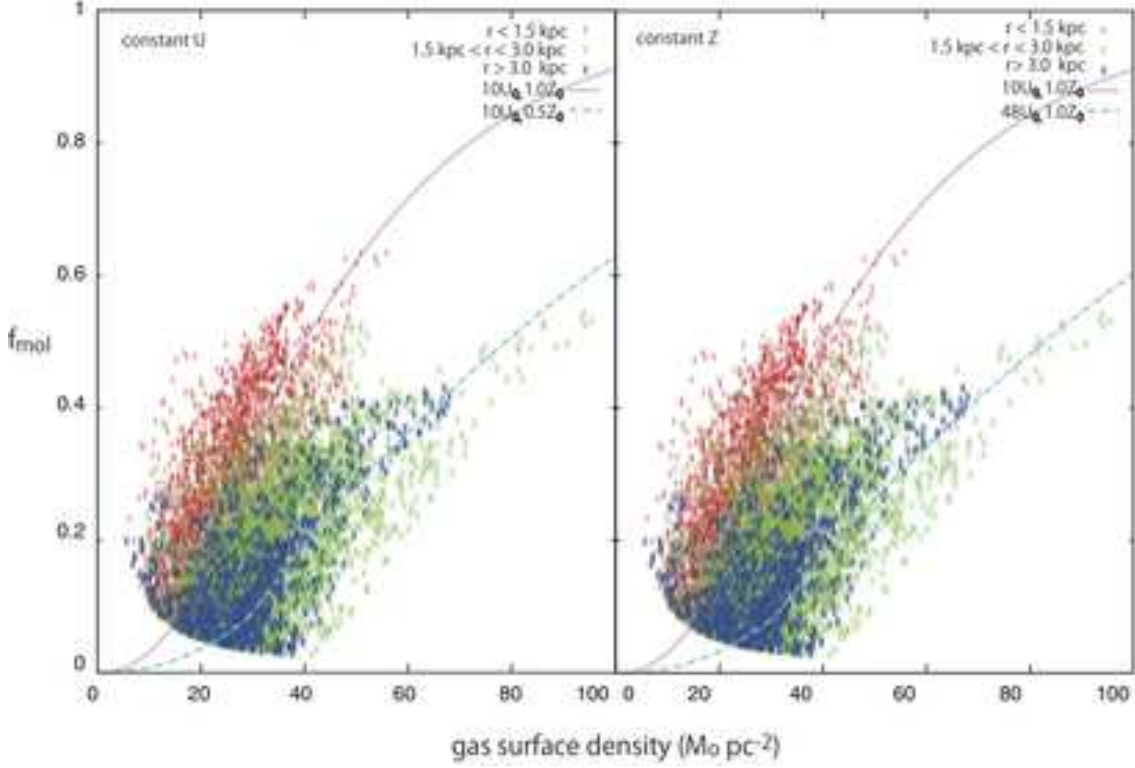
In fact, an early observational study on the metallicity distribution in M33 (Vilchez et al. 1988) suggests that there is a sharp increase in metallicity in the central <2.4 kpc region.
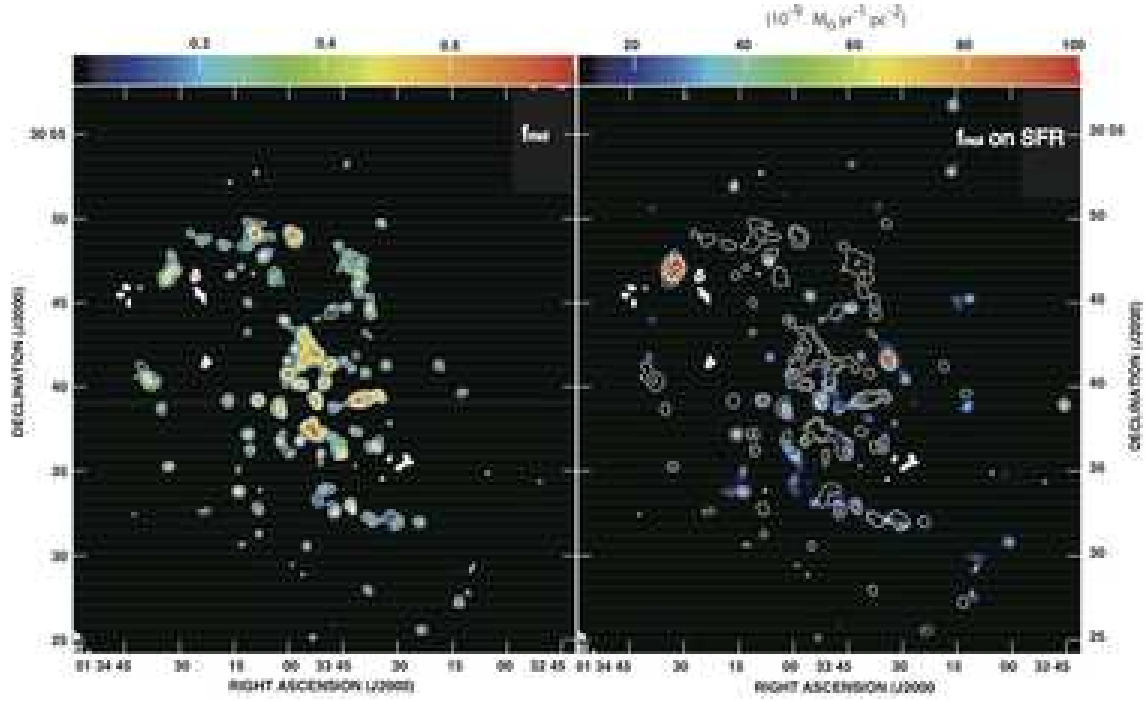
Fig. 5. Molecular fraction (f_{mol}) is shown with contours. Contour levels are 0.2, 0.4, and 0.6. Colors are f_{mol} in the left panel and SFR in the right panel.
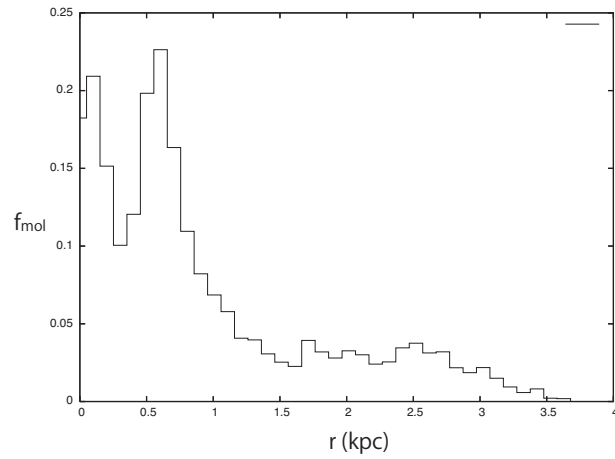
Fig. 6. Radial distribution of f_{mol}.

11

Fig. 7. Correlation between gas surface density and f_{mol}. Red, blue, and green points represent data with ranges of $r \leq 1.5$ kpc, 1.5 kpc $\leq r \leq 3$ kpc, and $r \geq 3$ kpc. Pink dotted and cyan dashed lines indicate correlation for $U = 10U_0$ at $Z = Z_0$ and $Z = 0.5Z_0$ (left), and for $Z = 1.0Z_0$ at $U = 10U_0$ and $U = 48Z_0$ (right), respectively.

Although the existence of a metallicity gradient within M33 is still under debate (Rosolowsky and Simon 2008), we suggest that the existence of a difference in Z between the inner and outer parts of M33 is a plausible explanation for the presence of two sequences in the $\Sigma_{\text{HI+H}_2} - f_{\text{mol}}$ diagram.

On the other hand, a difference in U between the inner and outer parts is needed to explain the two sequences if we assume that Z is constant across the galaxy. For example, we suggest that $U = 10U_0$ and $U = 50U_0$ for the inner and outer parts, respectively, if $Z = Z_0$ at all radii.

Is there any observational evidence for enhanced radiation field strength in the outer parts of M33? If the interstellar radiation field originates from massive stars, elevated star formation should be expected in the outer parts, but in reality, we see no such tendency, as shown in figure 4. Moreover, if this was the case, we could expect a smaller f_{mol} value for larger SFR, but again no such correlation is found (right panel in figure 5). It is possible for the strength of the interstellar radiation field to be determined by intermediate- and/or low-mass stars (e.g., Komugi et al. 2011), but again the strength of U does not account for the observed tendency of f_{mol}; a significant enhancement of U by a factor of 5 is needed in the outer disk,

which is inconsistent with the stellar distribution traced by K-band images. Considering these facts, we suggest that differences in the radiation field strength is not the cause for the presence of two sequences in the $\Sigma_{HI+H_2} - f_{mol}$ diagram. For the first possibility, therefore, the two observed distinct sequences can be explained by differences in Z between the inner and outer parts.

4.2. Overestimation of gas density

Next, we discuss the possibility that we are overestimating Σ_{HI+H_2} in the outer part. In figure 7, the value of the horizontal axis corresponds to the gas pressure, or volume density, n. n is given by the surface density Σ_{HI+H_2} multiplied by the scale height h, and here we assume that h is constant for all radii. Therefore, if there is a difference in h between the inner and outer parts of the galaxy, n values should be modified accordingly. For instance, if h is higher by a factor of 2 at the outer radii, n should be lower by the same factor. In this case, the value of the horizontal axis in figure 7 is overestimated by a factor of 2 and the true data points should be shifted to the left. If this is the case, the true $\Sigma_{HI+H_2}-f_{mol}$ correlation (after correction for overestimation caused by the differences if h) will show just a single sequence.

Is there any observational support for differences in h in M33? Although no direct measurement of h has been conducted for in M33, it has been pointed out that h is larger in the outer parts than in the inner region by a factor of two or more in the Milky Way (Nakanishi & Sofue 2006). Hence, we cannot reject this scenario as a possible cause of the two observed sequences.

It is worth noting that the variation in either metallicity or scale height is rather bimodal—not continuous. NIR observations have revealed the existence of an $r^{1/4}$ stellar distribution (or bulge) with a scale length of $8'$ or 2 kpc (Regan & Vogel 1994). The putative bulge size of 2 kpc is close to the threshold of these two sequences (~ 1.5 kpc), leading to a speculation that the different environments in and outside the bulge are the cause of the bimodality of the correlation.

4.3. Dynamical effect

Another possibility is a dynamical effect such as a shock compression of ISM due to spiral arms. For example, spiral density wave shocks may push the transition from warm neutral material to cold neutral atomic gas, or simply increased self-shielding to allow for the the formation of molecules. Such perturbations may be weaker in the outer parts of galaxies owning to the decrease in the stellar density and shallower spiral potentials. We suggest that this is indeed another possibility, although it may not be a major driver of the observed two sequences, because the strength of the spiral density wave in M33 is very weak as mentioned in previous section.

In summary, we have three plausible explanations for the two observed sequences in the $\Sigma_{HI+H_2}-f_{mol}$ diagram. The first is the enhanced molecular formation caused by higher

metallicity in the inner parts of M33. Another is the idea that two sequences are observed because of differences in the scale height of the gas disk between the inner and outer parts of M33, and the true $\Sigma_{\mathrm{HI}+\mathrm{H}_2}-f_{\mathrm{mol}}$ diagram (after correction for the overestimation of n) will show just a single correlation sequence. Dynamical effects such as compression of ISM due to spiral arms may also a possible cause.

5. Summary

We performed all-disk mapping of ^{12}CO ($J = 1$–0) in the nearby spiral galaxy M33 using the NRO 45-m telescope. The observed area covers the central $30' \times 30'$ (7.3 kpc $\times$ 7.3 kpc) of M33, including most of the famous HII regions such as NGC 604 and NGC 595. The spatial resolution of the resultant map is $19''.3$, corresponding to 81 pc, which is sufficient to identify each GMC in the disk.

Our conclusions are summarized as follows.

1. The total integrated intensity map of ^{12}CO ($J = 1$–0) emission shows a clumpy structure with a typical spatial scale of $\sim$100 pc, corresponding to GMCs. We find no diffuse, smoothly distributed components of molecular gas at this sensitivity.

2. The overall distribution of molecular gas roughly agrees with that of HI; that is, CO emission coincides with the peaks of HI emission in general. However, close inspection of the CO and HI maps suggests that not every CO emission is associated with local HI peaks, particularly in the inner portions of the disk ($r < 2$ kpc), although most of the CO emission is located at the local HI peaks in the outer parts.

3. We find that most of the uncovered GMCs are accompanied by massive star-forming regions, although the SFRs vary widely from cloud to cloud.

4. The azimuthally averaged HI gas surface density exhibits a flat radial distribution. However, the CO radial distribution shows a significant enhancement within the central 1–2 kpc region, which is very similar to that of the SFR. We find that HI is the dominant component compared with CO at all radii.

5. We obtained a map of molecular fraction, $f_{\mathrm{mol}} = \frac{\Sigma_{\mathrm{H}_2}}{\Sigma_{\mathrm{HI}}+\Sigma_{\mathrm{H}_2}}$, at a 100-pc resolution. This is the first such map covering an entire galaxy at GMC-scale resolution. We find that f_{mol} tends to be high in the inner region.

6. The correlation between f_{mol} and gas surface density was investigated. We found two distinct sequences in the correlation. The presence of two correlation sequences can be explained by differences in metallicity, i.e., higher metallicity in the central region ($r < 1.5$ kpc) than in the outer parts (a factor of $\sim$2). Alternatively, differences in scale height can also account for the two observed sequences, i.e., increased scale height toward the outer disk. Dynamical effects such as spiral shocks may also work.

References

Calzetti, D., et al. 2007, ApJ, 666, 870

Deul, E. R., & van der Hulst, J. M. 1987, A&AS, 67, 509

Elmegreen, B.G., 1989, ApJ, 338, 178

Elmegreen, B.G., 1993, ApJ, 411, 170

Engargiola, G., Plambeck, R. L., Rosolowsky, E., & Blitz, L. 2003, ApJS, 149, 343

Freedman, W. L., Wilson, C. D., & Madore, B. F. 1991, ApJ, 372, 455

Gratier, P., et al. 2010, A&A, 522, A3

Honma, M., Sofue, Y., & Arimoto, N. 1995, A&A, 304, 1

Hoopes, C. G., & Walterbos, R. A. M. 2000, ApJ, 541, 597

Heyer, M. H., Corbelli, E., Schneider, S. E., & Young, J. S. 2004, ApJ, 602, 723

Heyer, M., Krawczyk, C., Duval, J., & Jackson, J. M. 2009, ApJ, 699, 1092

Kawamura, A., et al. 2009, ApJS, 184, 1

Kennicutt, R. C., Jr. 1998, ApJ, 498, 541

Komugi, S., et al. 201, PASJ, 63, in press

Kramer, C., et al. 2010, A&A, 518, L67

Kuno, N., Nakai, N., Handa, T., & Sofue, Y. 1995, PASJ, 47, 745

Kuno, N., & Nakai, N. 1997, PASJ, 49, 279

Miura, R., et al. 2010, ApJ, 724, 1120

Nakanishi, H., Kuno, N., Sofue, Y., Sato, N., Nakai, N., Shioya, Y., Tosaki, T., Onodera, S., Sorai, K., Egusa, F., Hirota, A. 2006, ApJ, 651, 804

Nakanishi, H., & Sofue, Y. 2006, PASJ, 58, 847

Onodera, S., et al. 2010, ApJL, 722, L127

Rand, R. J., & Kulkarni, S. R. 1990, ApJL, 349, L43

Regan, M. W., & Vogel, S. N. 1994, ApJ, 434, 536

Rieke, G. H., et al. 2004, ApJS, 154, 25

Rosolowsky, E., Keto, E., Matsushita, S., Willner, S. P. 2007, ApJ, 661, 830

Rosolowsky, E., Simon, J. D. 2008, ApJ, 675, 1213

Sakamoto, K., Okumura, S. K., Ishizuki, S., & Scoville, N. Z. 1999, ApJ, 525, 691

Sanders, D. B., Scoville, N. Z., & Solomon, P. M. 1985, ApJ, 289, 373

Sawada, T., et al. 2008, PASJ, 60 445

Scoville, N. Z., & Sanders, D. B. 1987, Interstellar Processes, 134, 21

Sofue, Y., Honma, M., & Arimoto, N. 1995, A&A, 296, 33

Sunada, K., Yamaguchi, C., Nakai, N., Sorai, K., Okumura, S. K., Ukita, N. 2000, Proc. SPIE, 4015, 237

Tosaki, T., Miura, R., Sawada, T., Kuno, N., Nakanishi, K., Kohno, K., Okumura, S. K., & Kawabe, R. 2007, ApJL, 664, L27

Vilchez, J. M., Pagel, B. E. J., Diaz, A. I., Terlevich, E., & Edmunds, M. G. 1988, MNRAS, 235, 633

Waller, W. H., Clemens, D. P., Sanders, D. B., & Scoville, N. Z. 1987, ApJ, 314, 397

Wilson, C. D., & Scoville, N. 1989, ApJ, 347, 743

Wilson, C. D., & Scoville, N. 1990, ApJ, 363, 435